Edinburgh Research Explorer

The effects of strontium-doped bioactive glass and fluoride on hydroxyapatite crystallization

The effects of strontium-doped bioactive glass and fluoride on hydroxyapatite crystallization

Abstract

Objectives: This study investigated the effects of a new strontium-doped bioactive glass and fluoride on hydroxyapatite crystallization.

Methods: We designed an *in vitro* experiment with calcium phosphate ($CaCl_2 \cdot 2H_2O + K_2HPO_4$ in buffer solution) with different concentrations of strontium-doped bioactive glass (1mg/ml or 5mg/ml), and different concentrations of fluoride (0 ppm, 1 ppm or 5 ppm). Tris-buffered saline served as negative control. After incubation at 37°C for 48 hours, the shape and organization of crystals were examined by transmission electron microscopy (TEM) and electron diffraction. Structure of the crystals was assessed by powder X-ray diffraction (P-XRD) and unit cell parameters were calculated. Characterization of the crystals were performed by Raman spectroscopy and Fourier Transform Infrared Spectroscopy (FTIR).

Results: TEM and selected-area electron diffraction revealed that the precipitates in all experimental groups were crystalline apatite. There was an interaction between strontium and fluoride with different concentrations on crystal thickness ($p=0.008$). P-XRD indicated the formation of strontium-substituted-fluorohydroxyapatite and strontium-substituted-hydroxyapatite in the groups with both bioactive glass and fluoride. Expansion or contraction of crystal unit cell was influenced by the concentrations of strontium and fluoride. Raman spectra showed strong phosphate band at 960 cm^{-1} in all experimental groups and displayed no obvious shift. FTIR results confirmed the formation of apatite.

Conclusions: The results of this study suggest that strontium-doped bioactive glass and fluoride have synergistic effects on hydroxyapatite crystallization.

Clinical Significance: Strontium-doped bioactive glass and fluoride have synergistic effects on hydroxyapatite crystallization by producing strontium-substituted-hydroxyapatite and strontium-substituted-fluorohydroxyapatite with enhanced bioactivity and reduced solubility which could be beneficial for caries management.

Key words: bioactive glass, strontium, hydroxyapatite, fluorohydroxyapatite, mineral crystallization, caries

1. Introduction

Dental caries is one of the most common chronic diseases worldwide [1]. It is a biofilm-mediated disease which is associated with an imbalance between demineralization and remineralization, leading to mineral loss of dental hard tissues [2]. Mechanical tooth preparation is a destructive and irreversible method of removing the natural dental tissues and restored with artificial materials such as resin composite or glass ionomer cement. The restorative fillings are gradually worn out leaving space for the further development of lesions [3]. Contemporary caries management philosophy has changed from the traditional pure surgical approach to a medical model [4]. Minimal intervention with remineralizing therapy is suggested for management of caries. Fluoride therapies, with their well-known remineralizing properties, are generally considered the main reason for dental caries reduction in most populations [3, 5]. However, the currently available fluoride therapies still have limited efficacy in some individuals, and at the population level, the effect of fluoride in reducing caries prevalence is reaching a plateau. Moreover, young children take high concentration of fluoride products will be at risk of dental fluorosis [6]. Consequently, investigators have been developing new remineralizing therapies, especially bioactive materials, to enhance the effect of existing fluoride therapies, therefore to establish new strategy of caries management [4, 5].

Bioactive glass, such as Bioglass 45S5 (Na_2O-CaO-SiO_2-P_2O_5), has shown promising effect on reducing dentine hypersensitivity and promoting remineralization of carious tissues [7]. Studies have shown that bioactive glass particles can adhere to dentine and form a layer which is similar in composition to dentine, thereby blocking the dentinal tubules [8, 9]. Bioactive glass has been shown to increase microhardness of dentine caries lesion [10], possibly through formation of apatite on the tooth surface, thus having the potential to restore the mechanical properties of the tooth. Reaction of bioactive glass starts when exposed to artificial saliva or stimulated body fluid, followed by pH rise which can promote the precipitation of calcium phosphate on the surface of the bioactive glass and then an enrichment layer was formed to produce an apatite-like layer on the tooth surface [11]. Elevation in pH and the precipitation of dissolution products are conducive to calcium phosphate nucleation [12]. In addition, bioactive glass also has an antibacterial effect on cariogenic bacterial species, which is due to pH elevation and presence of antibacterial ions such as strontium [13, 14]. Adding strontium into toothpaste shows good dentine tubule occlusion and has been used to treat dentine hypersensitivity [15], and can lead to caries inhibition [16]. Recently, a new bioactive glass

(HX-BGC, SiO_2-P_2O_5-Na_2O-SrO) with addition of strontium was developed in order to merge the properties of Bioglass 45S5 and strontium [17, 18]. The atomic percentage of strontium in powder HX-BGC is around 1.6 % [17]. The new HX-BGC shows superior antibacterial ability by inhibiting acid producibility, suppressing the cariogenic bacteria growth [17] and can occlude the dentine tubules better than Bioglass 45S5 [18].

Mineral crystallization is a complex process. An *in vitro* study has shown that bioactive glass particles can form a hydroxycarbonate apatite layer on dentine [9]. Calcium and phosphate ions in saliva are the major mineral sources in the oral environment. The contribution of calcium, phosphate, and hydroxyl ions present in saliva to apatite deposition is fundamental. However, there are very few studies on how bioactive glass reacts with salivary components regarding the apatite crystallization process. Incorporating fluoride into the apatite structure of dental hard tissue can inhibit the progress of lesion development by reducing solubility of hard tissue under acid challenge [19-22]. A synergistic effect between strontium and a low concentration of fluoride in caries prevention has been reported [23]. Therefore, this new bioactive glass with addition of strontium is expected to have synergistic effect with fluoride on mineralization. The aims of this study were: 1) to investigate the effect of Strontium (Sr)-doped bioactive glass in apatite formation, and 2) to investigate the effect of Sr-doped bioactive glass in apatite formation with the presence of fluoride. A simplified chemical model was used. The null hypotheses tested were that: 1) Sr-doped bioactive glass has no effect on apatite formation, and 2) combination of Sr-doped bioactive glass and fluoride has no effect on apatite formation.

2. Materials and Methods

2.1 Mineralization reaction

HX-BGC used in this reaction has been developed and described above and it has a composition of SiO_2, P_2O_5, Na_2O and SrO which was elaborated in our previous study [17]. The reaction was performed in a Tris-buffered saline (TBS) consisting of a 50mM Trizma base and 150mM sodium chloride (NaCl) in Milli-Q water set at pH 7.4. Apatite formation was conducted in TBS by incubating $CaCl_2$ (5.88mM) with K_2HPO_4 (4.12mM) at 37°C, in the presence or absence of HX-BGC and sodium fluoride (NaF) with different concentration. $CaCl_2$ and K_2HPO_4 were added into TBS and completely stirring, followed by transferring to the reaction tubes, incubated with different concentrations of HX-BGC and NaF at 37°C for 48h. There were 6 experimental groups containing HX-BGC: (1) HX-BGC 1mg/ml (B1); (2)

HX-BGC 1mg/ml + 1 ppm fluoride (B1F1); (3) HX-BGC 1mg/ml + 5 ppm fluoride (B1F5); (4) HX-BGC 5mg/ml (B5); (5) HX-BGC 5mg/ml + 1 ppm fluoride (B5F1); (6) HX-BGC 5mg/ml + 5ppm fluoride (B5F5). One group acted as control and it contained $CaCl_2.2H_2O$ + K_2HPO_4 in TBS with no HX-BGC nor NaF. After incubation for 48 h, samples were collected from the suspensions. 10μl of each suspension were collected on the copper grids and analyzed with transmission electron microscopy (TEM) with selected-area electron diffraction (SAED) and energy-dispersive X-ray spectroscopy (EDS), as described below. The rest was used to obtain powder samples and divided into three parts. They were collected after centrifugation and evaporation for powder X-ray diffraction (P-XRD), Raman spectroscopy and Fourier transform infrared spectroscopy (FTIR) assessment. Three specimens from each HX-BGC groups and control were used, the whole experiment was done in triplicate.

2.2 Transmission Electron Microscopy Analysis

For preparing samples, formvar carbon coated 400-mesh copper grids were used and 10μl of each suspension sample was collected, and dropped on the grids and air dried. TEM analysis of the samples from the 7 experimental groups was conducted by transmission electron microscopy (TEM, Tecnai G2 20 S-TWIN, FEI, United States) equipped with a Gatan CCD camera (2.7 × 2.7k pixel) and X-Max 80T energy-dispersive X-ray spectroscopy (EDS) detector. Selected-area electron diffraction (SAED) was performed to confirm the crystallographic parameters of the study samples. The chemical composition of the deposits was characterized and the ratios quantified by EDS. Length and width of apatite crystals were measured by ImageJ (National Institutes of Health, Bethesda, MD, USA).

2.3 Powder X-ray Diffraction

The powder samples were collected and washed by deionized water for the first two times and by ethanol for the last time, followed by removing the ethanol and waited for evaporation to collect the pure powder. The powder samples were assessed with X-ray diffractometer (Rigaku SmartLab 9kW, Tokyo, Japan) equipped with a CuKα lamp (λ = 1.54056 Å). The parameters for collecting data were: 2θ range=20º to 60º, step size=0.02º and scan speed=0.6 s/step. Bragg's equation was used to calculate the d-spacing (interplanar distance), from the (300) and (002) reflections observed in the XRD patterns:

$$d = \frac{n\lambda}{2sin\theta}$$

where d represents interplanar distance, n represents a consecutive natural number, λ is the wavelength, and θ represents the incident angle of the X-ray beam. The lattice parameters ($a=b$ and c) of the hexagonal unit cell were calculated by the following equation:

$$\frac{1}{d^2} = \frac{4}{3}\left(\frac{h^2 + hk + k^2}{a^2}\right) + \frac{l^2}{c^2}$$

where d represents the interplanar distance; h, k and l represent the Miller indices; and a and c represent the lattice constants. Jade 6 (MDI, California, United States) was used to analyze the phase of the patterns.

2.4 Raman Spectroscopy

Powder samples from the 7 experimental groups were collected and put on the cover slips, then optically characterized on a scanning confocal microscopy system integrated with a monochromator + CCD detector for Raman spectroscopy (WITec GmbH, Ulm, Germany). A 514.5 nm argon ion laser (Melles Griot) was used as the excitation source throughout this assessment. Each powder sample was put on a glass slide to obtain the spectrum. Three 50s spectra were taken between Raman wavenumber shifts from 400 to 1,600 cm^{-1}.

2.5 Fourier Transform Infrared Spectroscopy

Powder samples from the 7 experimental groups were prepared with potassium bromide (KBr) to form a disk using a matched mold of Bruker Tensor 27 Spectrometer (Germany), which had a spectral range (7,500 - 370 cm^{-1}) with standard KBr beam-splitter. Subsequently, the sample discs were separately assessed by the FTIR spectrometer from 500 to 4,000 cm^{-1}.

2.6 Statistical Analysis

Shapiro-Wilk test for normality was used to evaluate the length and width of the apatite crystals. The differences between groups were assessed by one-way analysis of variance (ANOVA) with Bonferroni post doc tests. The interaction effect between HX-BGC and fluoride with different concentrations on crystal size was assessed by two-way ANOVA. All data analyses were conducted by using IBM SPSS Statistics 25. The statistical significance level was set at 0.05.

3. Results

3.1 TEM, SAED and EDS result

Figure 1 shows the TEM and SAED images, and EDS result of the 7 experimental groups. The morphology of the apatite crystals formed in the absence of HX-BGC and fluoride was plate-shaped (Figure 1-A), while SAED showed the typical reflections corresponding to the (211), (002), and (102) planes of apatite, and EDS confirmed the presence of calcium and phosphorus [24]. The addition of HX-BGC and fluoride with different concentrations led to a different morphology of the formed apatite crystals compared to that seen in the calcium phosphate control group. A ribbon and plate-shape morphology was observed with the presence of HX-BGC (Figure 1-C, I), while tip-ended prismatic morphology with shaper edges was observed with the presence of both HX-BGC and fluoride (Figure 1-E, G, K, M). SAED patterns confirmed the crystals were apatite. EDS spectra revealed the presence of calcium and phosphorus in each group, with an additional signal attributed to strontium in the groups with HX-BGC. The presence of fluoride was detected in the B1F5 and B5F5 groups (Figure 1-H, N).

Table 1 illustrates the length and width of the 7 experimental groups. The largest crystal size ($p<0.001$) was 227.7±22.4 nm found in the group with 5mg/ml HX-BGC and 5ppm fluoride (group B5F5). When both HX-BGC and fluoride were present, the interaction between these two significantly influenced the width of the crystals ($p=0.008$) but not the length ($p=0.731$). As the concentration of HX-BGC and fluoride increased, the crystals became wider. The interaction effect of HX-BGC (1mg/ml and 5mg/ml) and 5ppm fluoride on the width of crystals was the strongest ($p=0.009$) (Figure 2).

3.2 Phase analysis and lattice parameters reflected from the P-XRD pattern

Figure 3 shows the typical P-XRD patterns of the 7 experimental groups. The P-XRD analysis indicated the solid deposited in the calcium phosphate control group scattered X-rays similar to hydroxyapatite (JCPDS No. 73-0293). The reflections were sharper in the 6 experimental groups with bioactive glass than in the control group. In the two groups with HX-BGC only (group B1 and B5), the (002) reflection was not significantly changed, while the (300) reflections shifted from 32.95º (2θ) in the control to 32.87º (2θ) in group B1 and to 32.86º (2θ) in group B5. This pattern of reflection indicated the formation of Sr-substituted-hydroxyapatite ($Ca_{10-x}Sr_x(PO_4)_6(OH)_2$, $0<x<10$, x increase with Sr concentration) [25]. This shift also reflected the increase of the calculated unit cell parameters (Table 2). With addition of fluoride, the

reflections indicated formation of Sr-substituted hydroxyapatite ($Ca_{10-x}Sr_x(PO_4)_6(OH)_2$), Sr-substituted-fluorohydroxyapatite ($Ca_{10-y}Sr_y(PO_4)_6(OH)_{2-x}F_x$, $0<y<10$, $0<x<1$) in groups B1F1, B1F5, B5F1 and B5F5. In addition, a new phase with acidic phosphate ions named calcium hydrogen phosphate hydroxide ($Ca_9HPO_4(PO_4)_5OH$, JCPDS No. 46-0905) appeared in the B5F1 and B5F5 samples.

3.3 Raman spectroscopy

Figures 4 shows the Raman shift of the samples from the 7 experimental groups. The strongest active ν_1 PO_4 peak appeared in all groups at around 960 cm^{-1} in the spectra. The ν_3 PO_4 mode appeared as relatively sharp band at around 1122 cm^{-1} in the spectra of all samples [26]. There was an additional peak at around 879 cm^{-1} in groups B5F1 and B5F5, which was attributed to the acidic phosphate ions (HPO_4^{2-}) [27]. This phenomenon further proved the presence of the new phase mentioned in the analysis of XRD result. The ν_2 domain of all the samples were nearly the same, showed an asymmetric band in the region of bands around 423 to 432 cm^{-1} in the spectra. The most obvious peak appeared around band at 426 cm^{-1} of the spectra. Similarly, the ν_4 mode showed three main bands with constant wavenumber (578 cm^{-1}, 586 cm^{-1}, 590 cm^{-1}) in the spectra, with the band at 590 cm^{-1} exhibited the strongest intensity. The abovementioned peak exhibition was consistent with findings of previous studies [26, 27]

3.4 FTIR

Figure 5 shows the FTIR spectrum of the 7 experimental groups. The absorption bands sited at 962 and 1032 cm^{-1} were attributed to the characteristic of phosphate (PO_4^{3-}) in the experimental groups. The absorption peaks at 1463 and 1415 cm^{-1} were attributed to the stretching vibrations of carbonate (CO^{3-}), which derived from carbon dioxide from surrounding atmosphere that was mixed in the reaction during mixing, and incorporated into the crystal structure [28]. We associate the peak at 875 cm^{-1} in the spectra with HPO_4^{2-} which was consistent with the Raman peak at 879 cm^{-1} in the samples B5F1 and B5F5 (Figure 4) and as described in another study [29]. It was noted that the calcium phosphate control group showed an absorption peak at 865 cm^{-1} of the spectra which may attributed to CO^{3-} group. The intensity of carbonate peaks was higher in the groups with higher strontium concentration. There were two absorption bands sited at 1640 cm^{-1} and 3445 cm^{-1} related to the O-H bond. The absorption peaks mentioned above confirmed the presence of hydroxyapatite and fluorohydroxyapatite, which was similar to the results reported previously [30, 31].

4. Discussion

This study aimed to investigate the effect of Sr-doped bioactive glass and fluoride in apatite crystal formation during mineralization. In this study, it was found that the strontium from the bioactive glass and fluoride enabled the formation of Sr-substituted-hydroxyapatite and Sr-substituted-fluorohydroxyapatite, which depended on the concentrations of strontium and fluoride. Therefore, the two null hypotheses of this study were rejected.

A previous study has reported the effect of fluoride on the formation of fluoride-substituted hydroxyapatite [22]. A fairly well-ordered fluorohydroxyapatite deposited and it was found to be more chemically stable due to replacing action of the related ions (OH^- substituted by F^-). The formed fluorohydroxyapatite with lower solubility may favor arrest of carious lesion of teeth [22]. Therefore, here we paid more attention on the effect of the combination of Sr-doped bioactive glass and fluoride. Due to its chemical similarity to calcium, strontium can be incorporated into the crystal lattice of hydroxyapatite. Sr-hydroxyapatite has good bioactivity and can directly bond to bony tissue even though under no weight-bearing condition [32]. Apart from biological properties, previous studies on bioactive glasses found an increase in fluoride release in the presence of strontium due to the strontium-caused expanded and more degradable network can be more preferential for fluoride release, and that there was a synergistic effect of strontium and fluoride on hydroxyapatite formation [33, 34]. Other studies reported that incorporation of strontium and fluoride into the hydroxyapatite crystal reduced the dissolution of low- and high-carbonated hydroxyapatite [35], and strontium aided rehardening carious lesion in the presence of fluoride [20]. In the present study, there were two main crystallization phases in the hydroxyapatite formed in the presence of strontium and fluoride. The first phase is Sr-substituted-hydroxyapatite. This material has been shown to be chemically more stable than hydroxyapatite, particularly with the presence of fluoride [36, 37] and to have better bioactivity and greater ability to induce apatite precipitation than hydroxyapatite [32, 38]. Another phase is Sr-substituted-fluorohydroxyapatite which has increased thermal and chemical stability when compared with hydroxyapatite [22]. Thus, the addition of strontium into bioactive glass can lead to formation of apatites that are more resistant to dissolution with the presence of fluoride.

It is plausible that the lower 2θ values found in the XRD patterns in the B1 and B5 groups, indicating that the interplanar distances and lattice parameters were augmented (Table 2), are due to the presence of strontium in the lattice. In the reaction with TBS, Sr^{2+} from HX-BGC substituted some of the Ca^{2+} in the hydroxyapatite formed and expanded the unit cell which is in agreement with the larger strontium ionic radius (Ca^{2+}: 0.94Å, Sr^{2+}: 1.16Å) [34, 39-41]. This finding also agrees with those of previous studies. In one study, the lattice parameters increased linearly with the addition of strontium [25]. This is because strontium contains more electrons than calcium which causes more scattering of X-rays. Another study reported that with increasing percentage of strontium incorporated into apatite, there was an expansion of unit cell along the (002) plane [40]. This enlarged lattice can lead to preferential incorporation of fluoride over carbonate in the hydroxyapatite in the oral environment [35]. Hydroxyl ions in hydroxyapatite can be partially or completely replaced by fluoride ions during the mineralization reaction. The isotropic distribution of charge on fluoride ions results in a better fit in the lattice as compared with the larger asymmetric hydroxyl ions. This alternate arrangement produces a fairly well-ordered apatite structure, which is characterized with increased thermal and chemical stability when compared with hydroxyapatite [22]. Since F^- has an ionic radius smaller than that of OH^- (F^-: 1.33Å, OH^-: 1.52Å) [22], this explains the contraction of unit cell in the B1F5 and B5F5 groups with high fluoride concentration in this study.

Raman spectroscopy and FTIR are two common methods for confirming presence of apatite. In this study, the most obvious phosphate peak (v_1 PO_4) in the 900-1000 cm^{-1} region in Raman spectroscopy is consistent with apatite, either hydroxyapatite or fluoride/Sr-substituted apatite. With an increase in concentration of fluoride, there will be more fluoride ion substitution for hydroxyl ions, leading to an increase in the vibrational frequency of the v_1 PO_4 band [22]. Strontium with increasing percentage incorporated into apatite can influence shifting of the v_1 PO_4 band around 960 cm^{-1} [25]. However, a previous study reported that the phosphate groups of apatite mainly interacted with themselves and the substituted ions did not significantly change the phosphate band in the spectrum [42]. Thus, despite having some hydroxyl ions and calcium ions substituted, the phosphate bands remained in the fixed region. Result of this study is consistent with the finding in the abovementioned study. In addition, the v_2 phosphate mode exhibits two wavenumber positions and v_4 domain of phosphate modes always exhibits three main bands in the spectra [27, 43]. In this study, the two domains of phosphate modes also

appeared in the identical range of wavenumbers without significant shift. A study reported that carbonate bands were enhanced with an increased incorporation of strontium into bioactive glass [31], which is consistent with the FTIR finding of this study. This can explain why the split carbonate bands at 1463 and 1415 cm^{-1} were strengthened in this study.

In the groups with HX-BGC, enlarged apatite crystal size was observed by TEM. Similar results were reported by previous studies on synthetic apatite, which found an increase in strontium incorporation was accompanied by an increase in the size of crystals [31, 44]. This is likely due to the substitution of calcium by strontium. Fluoride ion substitution for hydroxyl ions can reduce lattice microstrain and thus enable fluorohydroxyapatite crystals to form larger particles [22, 45]. However, low fluoride concentrations were used in this study and the amount of fluoride ion substitution should not be significant. Therefore, it is plausible that strontium content is the dominant factor in influencing the crystal size in this study. Replacement of calcium by strontium provokes lattice strain and having strontium in the hydroxyapatite lattice can impose a distortion to the structural arrangement and affect crystal symmetry [41]. A study showed a 25% strontium substitution caused structural asymmetry [40]. It should be noted that the concentration of strontium in this study was at a relatively low level, which should not have a high risk of distortion in the structure of the formed apatite. In addition, a relatively low percentage of fluoride substitution can increase the stability of the structure and reduce the lattice strain [22, 40]. Thus, a hexagonal structure was likely maintained.

In this study, a neutralized buffered calcium phosphate solution was adopted to conduct the mineralization reaction. It is a simple chemical buffered system which is able to initiate the precipitation of amorphous calcium phosphate, followed by transforming the depositions into apatite crystals [22]. However, this chemical model lacks the ability to stimulate the real situation in the mouth. It is difficult for this *in vitro* system without biological components to simulate the complex *in vivo* situation of the oral cavity. The process of remineralization using bioactive glass includes exchanging ions (Na^+, Ca^{2+}, PO_4^{3-}, Sr^{2+}) in the silicate network with the surrounding oral liquid to supersaturate the ions in the fluid, which then precipitate on the demineralized dental tissue [46]. Saliva has good buffering capacity in maintaining pH due to the presence of three buffer systems (carbonic acid/bicarbonate system, phosphate system, and protein system). Both calcium and phosphate are the essential ions in the nucleation of hydroxyapatite. Acidic micro-environment can induce the dissolution of tooth minerals and the release of hydroxyl ions, which promote the exchange of fluoride ions for hydroxyl ions [22].

In this study, the calcium and phosphate ions were provided by incubating $CaCl_2$ with K_2HPO_4 in the Tris buffer, which was a simulation of saliva for the basic reaction of apatite formation. Further studies are needed to investigate the use of Sr-doped bioactive glass to promote mineralization in bone and dental tissues. High quality clinical trials are required to evaluate its potential use and provide the necessary clinical evidence before making a firm recommendation.

5. Conclusion

The results of this study suggest that Sr-doped bioactive glass and fluoride have effects on apatite formation by producing Sr-substituted-hydroxyapatite and Sr-substituted-fluorohydroxyapatite. Strontium and fluoride incorporated into hydroxyapatite crystals can enhance the bioactivity and stability of these formed apatites, which could be beneficial for caries management.

Reference

[1] C.H. Chu, M.L. Mei, E.C.M. Lo, Use of fluorides in dental caries management, General dentistry 58(1) (2010) 37-43.

[2] R.H. Selwitz, A.I. Ismail, N.B. Pitts, Dental caries, Lancet (London, England) 369(9555) (2007) 51-9.

[3] F. Schwendicke, J.E. Frencken, L. Bjorndal, M. Maltz, D.J. Manton, D. Ricketts, K. Van Landuyt, A. Banerjee, G. Campus, S. Domejean, M. Fontana, S. Leal, E. Lo, V. Machiulskiene, A. Schulte, C. Splieth, A.F. Zandona, N.P. Innes, Managing Carious Lesions: Consensus Recommendations on Carious Tissue Removal, Adv Dent Res 28(2) (2016) 58-67.

[4] N.P.T. Innes, C.H. Chu, M. Fontana, E.C.M. Lo, W.M. Thomson, S. Uribe, M. Heiland, S. Jepsen, F. Schwendicke, A Century of Change towards Prevention and Minimal Intervention in Cariology, Journal of dental research 98(6) (2019) 611-617.

[5] N.B. Pitts, D.T. Zero, P.D. Marsh, K. Ekstrand, J.A. Weintraub, F. Ramos-Gomez, J. Tagami, S. Twetman, G. Tsakos, A. Ismail, Dental caries, Nature reviews. Disease primers 3 (2017) 17030.

[6] C. Gonzalez-Cabezas, C.E. Fernandez, Recent Advances in Remineralization Therapies for Caries Lesions, Adv Dent Res 29(1) (2018) 55-59.

[7] J.R. Jones, Review of bioactive glass: from Hench to hybrids, Acta Biomater 9(1) (2013) 4457-86.

[8] A.P. Forsback, S. Areva, J.I. Salonen, Mineralization of dentin induced by treatment with bioactive glass S53P4 in vitro, Acta Odontol Scand 62(1) (2004) 14-20.

[9] D.G. Gillam, J.Y. Tang, N.J. Mordan, H.N. Newman, The effects of a novel Bioglass dentifrice on dentine sensitivity: a scanning electron microscopy investigation, J Oral Rehabil 29(4) (2002) 305-13.

[10] Q. Wu, M.L. Mei, X. Wu, S. Shi, Y. Xu, C.H. Chu, Y. Chen, Remineralising effect of 45S5 bioactive glass on artificial caries in dentine, BMC oral health 20(1) (2020) 49.

[11] L.L. Dai, M.L. Mei, C.H. Chu, E.C.M. Lo, Mechanisms of Bioactive Glass on Caries Management: A Review, Materials 12(24) (2019).

[12] X. Li, J. Wang, A. Joiner, J. Chang, The remineralisation of enamel: a review of the literature, J Dent 42 Suppl 1 (2014) S12-20.

[13] J. Liu, S.C. Rawlinson, R.G. Hill, F. Fortune, Strontium-substituted bioactive glasses in vitro osteogenic and antibacterial effects, Dental materials : official publication of the Academy of Dental Materials 32(3) (2016) 412-22.

[14] D. Zhang, O. Lepparanta, E. Munukka, H. Ylanen, M.K. Viljanen, E. Eerola, M. Hupa, L. Hupa, Antibacterial effects and dissolution behavior of six bioactive glasses, J Biomed Mater Res A 93(2) (2010) 475-83.

[15] R.C. Olley, P. Pilecki, N. Hughes, P. Jeffery, R.S. Austin, R. Moazzez, D. Bartlett, An in situ study investigating dentine tubule occlusion of dentifrices following acid challenge, J Dent 40(7) (2012) 585-93.

[16] B. Czarnecka, J.W. Nicholson, Ion release by resin-modified glass-ionomer cements into water and lactic acid solutions, J Dent 34(8) (2006) 539-43.

[17] L.L. Dai, M.L. Mei, C.H. Chu, E.C.M. Lo, Antibacterial effect of a new bioactive glass on cariogenic bacteria, Archives of oral biology 117 (2020) 104833.

[18] Y. Zhong, J. Liu, X. Li, W. Yin, T. He, D. Hu, Y. Liao, X. Yao, Y. Wang, Effect of a novel bioactive glass-ceramic on dentinal tubule occlusion: an in vitro study, Aust Dent J 60(1) (2015) 96-103.

[19] N.R. Mohammed, N.W. Kent, R.J.M. Lynch, N. Karpukhina, R. Hill, P. Anderson, Effects of Fluoride on in vitro Enamel Demineralization Analyzed by F-19 MAS-NMR, Caries Research 47(5) (2013) 421-428.

[20] F. Lippert, The effects of fluoride, strontium, theobromine and their combinations on caries lesion rehardening and fluoridation, Archives of Oral Biology 80 (2017) 217-221.

[21] C.J. Tredwin, A.M. Young, E.A. Abou Neel, G. Georgiou, J.C. Knowles, Hydroxyapatite, fluor-hydroxyapatite and fluorapatite produced via the sol-gel method: dissolution behaviour and biological properties after crystallisation, Journal of materials science. Materials in medicine 25(1) (2014) 47-53.

[22] M.L. Mei, F. Nudelman, B. Marzec, J.M. Walker, E.C.M. Lo, A.W. Walls, C.H. Chu, Formation of Fluorohydroxyapatite with Silver Diamine Fluoride, J Dent Res 96(10) (2017) 1122-1128.

[23] G.H. Yassen, F. Lippert, G. Eckert, J. Eder, A.F. Zandona, The effect of strontium and combinations of strontium and fluoride on the remineralization of artificial caries lesions in vitro, Quintessence International 43(7) (2012) e95-e103.

[24] T. Kokubo, H.M. Kim, M. Kawashita, Novel bioactive materials with different mechanical properties, Biomaterials 24(13) (2003) 2161-75.

[25] M.D. O'Donnell, Y. Fredholm, A. de Rouffignac, R.G. Hill, Structural analysis of a series of strontium-substituted apatites, Acta Biomater 4(5) (2008) 1455-64.

[26] A. Antonakos, E. Liarokapis, T. Leventouri, Micro-Raman and FTIR studies of synthetic and natural apatites, Biomaterials 28(19) (2007) 3043-54.

[27] G. Penel, G. Leroy, C. Rey, E. Bres, MicroRaman spectral study of the PO4 and CO3 vibrational modes in synthetic and biological apatites, Calcif Tissue Int 63(6) (1998) 475-81.

[28] F. Mohandes, M. Salavati-Niasari, M. Fathi, Z. Fereshteh, Hydroxyapatite nanocrystals: simple preparation, characterization and formation mechanism, Mater Sci Eng C Mater Biol Appl 45 (2014) 29-36.

[29] L. Robinson, K. Salma-Ancane, L. Stipniece, B.J. Meenan, A.R. Boyd, The deposition of strontium and zinc Co-substituted hydroxyapatite coatings, J Mater Sci Mater Med 28(3) (2017) 51.

[30] M. Karimi, M.R. Ramsheh, S.M. Ahmadi, M.R. Madani, M. Shamsi, R. Reshadi, F. Lotfi, Reline-assisted green and facile synthesis of fluorapatite nanoparticles, Mater Sci Eng C Mater Biol Appl 77 (2017) 121-128.

[31] Z.Y. Li, W.M. Lam, C. Yang, B. Xu, G.X. Ni, S.A. Abbah, K.M. Cheung, K.D. Luk, W.W. Lu, Chemical composition, crystal size and lattice structural changes after incorporation of strontium into biomimetic apatite, Biomaterials 28(7) (2007) 1452-60.

[32] G.X. Ni, K.Y. Chiu, W.W. Lu, Y. Wang, Y.G. Zhang, L.B. Hao, Z.Y. Li, W.M. Lam, S.B. Lu, K.D. Luk, Strontium-containing hydroxyapatite bioactive bone cement in revision hip arthroplasty, Biomaterials 27(24) (2006) 4348-55.

[33] Y.C. Fredholm, N. Karpukhina, D.S. Brauer, J.R. Jones, R.V. Law, R.G. Hill, Influence of strontium for calcium substitution in bioactive glasses on degradation, ion release and apatite formation, Journal of the Royal Society, Interface 9(70) (2012) 880-9.

[34] D. Sriranganathan, N. Kanwal, K.A. Hing, R.G. Hill, Strontium substituted bioactive glasses for tissue engineered scaffolds: the importance of octacalcium phosphate, Journal of materials science. Materials in medicine 27(2) (2016) 39.

[35] J.D. Featherstone, C.P. Shields, B. Khademazad, M.D. Oldershaw, Acid reactivity of carbonated apatites with strontium and fluoride substitutions, J Dent Res 62(10) (1983) 1049-53.

[36] E. Lynch, D.S. Brauer, N. Karpukhina, D.G. Gillam, R.G. Hill, Multi-component bioactive glasses of varying fluoride content for treating dentin hypersensitivity, Dental materials : official publication of the Academy of Dental Materials 28(2) (2012) 168-78.

[37] A. D'Onofrio, N.W. Kent, S.A. Shahdad, R.G. Hill, Development of novel strontium containing bioactive glass based calcium phosphate cement, Dental materials : official publication of the Academy of Dental Materials 32(6) (2016) 703-12.

[38] W. Xue, J.L. Moore, H.L. Hosick, S. Bose, A. Bandyopadhyay, W.W. Lu, K.M. Cheung, K.D. Luk, Osteoprecursor cell response to strontium-containing hydroxyapatite ceramics, J Biomed Mater Res A 79(4) (2006) 804-14.

[39] X. Wu, G. Meng, S. Wang, F. Wu, W. Huang, Z. Gu, Zn and Sr incorporated 64S bioglasses: Material characterization, in-vitro bioactivity and mesenchymal stem cell responses, Mater Sci Eng C Mater Biol Appl 52 (2015) 242-50.

[40] C. Bussola Tovani, A. Gloter, T. Azais, M. Selmane, A.P. Ramos, N. Nassif, Formation of stable strontium-rich amorphous calcium phosphate: Possible effects on bone mineral, Acta biomaterialia 92 (2019) 315-324.

[41] J. Zeglinski, M. Nolan, M. Bredol, A. Schatte, S.A. Tofail, Unravelling the specific site preference in doping of calcium hydroxyapatite with strontium from ab initio investigations and Rietveld analyses, Phys Chem Chem Phys 14(10) (2012) 3435-43.

[42] G. Penel, G. Leroy, C. Rey, B. Sombret, J. Huvenne, E. Bres, Infrared and Raman microspectrometry study of fluor-fluor-hydroxy and hydroxy-apatite powders, Journal of Materials Science: Materials in Medicine 8(5) (1997) 271-276.

[43] H.O. Simila, N. Karpukhina, R.G. Hill, Bioactivity and fluoride release of strontium and fluoride modified Biodentine, Dental materials : official publication of the Academy of Dental Materials 34(1) (2018) e1-e7.

[44] O. Kaygili, S. Keser, M. Kom, Y. Eroksuz, S.V. Dorozhkin, T. Ates, I.H. Ozercan, C. Tatar, F. Yakuphanoglu, Strontium substituted hydroxyapatites: Synthesis and determination of their structural properties, in vitro and in vivo performance, Mater Sci Eng C Mater Biol Appl 55 (2015) 538-46.

[45] L.M. Rodriguez-Lorenzo, J.N. Hart, K.A. Gross, Influence of fluorine in the synthesis of apatites. Synthesis of solid solutions of hydroxy-fluorapatite, Biomaterials 24(21) (2003) 3777-85.

[46] D. Fernando, N. Attik, N. Pradelle-Plasse, P. Jackson, B. Grosgogeat, P. Colon, Bioactive glass for dentin remineralization: A systematic review, Materials science & engineering. C, Materials for biological applications 76 (2017) 1369-1377.
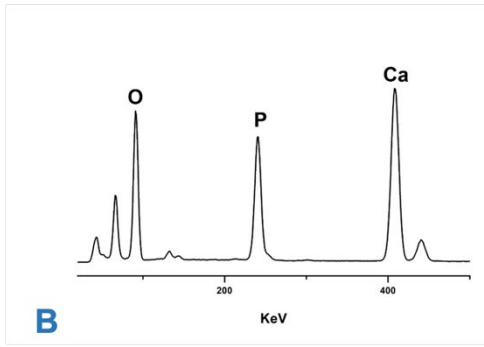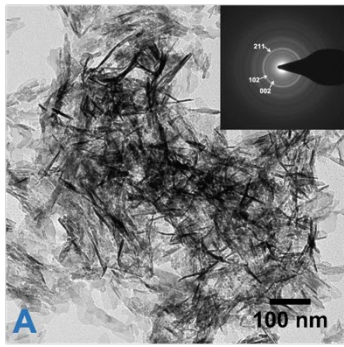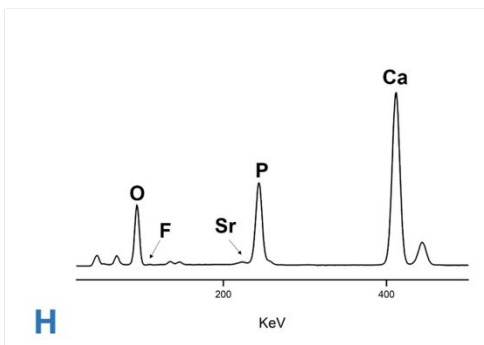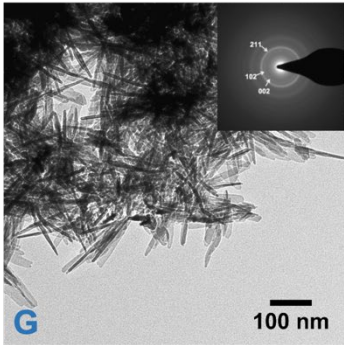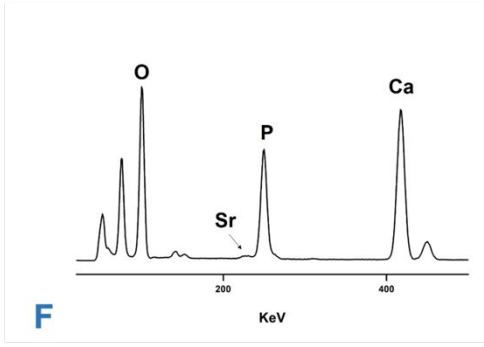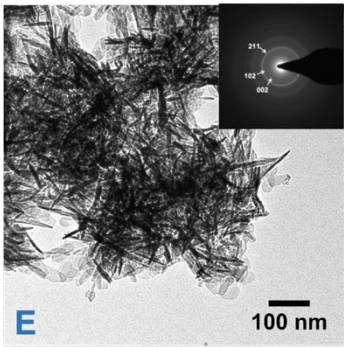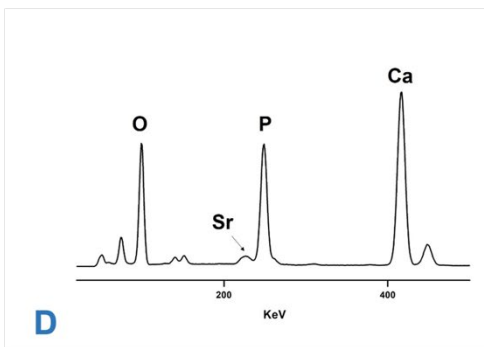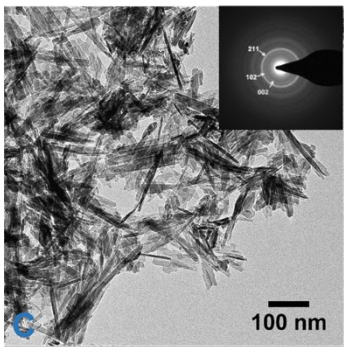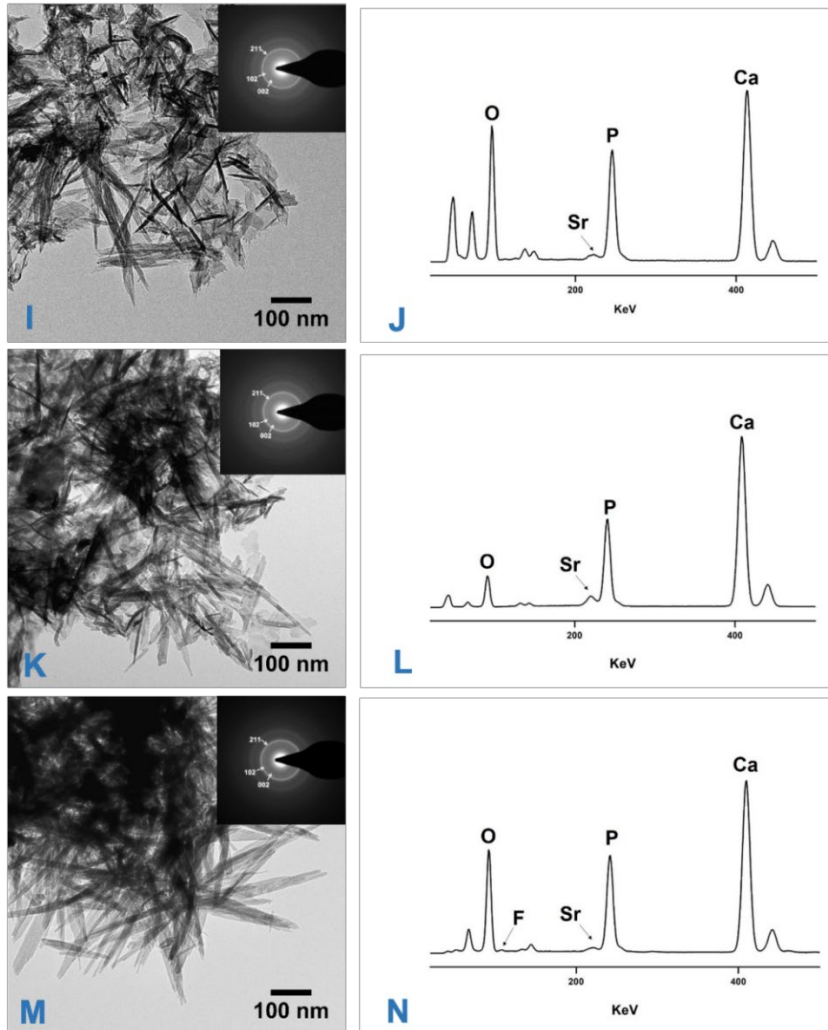
Figure 1 (Ⅰ: TBS group, Ⅱ: B1 groups and Ⅲ: B5 groups). Transmission electron microscopy data of experimental groups. TBS group: (A) morphology and SAED pattern, (B) EDS spectra. B1 group: (C) morphology and SAED pattern, (D) EDS spectra. B1F1 group: (E) morphology and SAED pattern, (F) EDS spectra. B1F5 group: (G) morphology and SAED pattern, (H) EDS spectra. B5 group: (I) morphology and SAED pattern, (J) EDS spectra. B5F1 group: (K) morphology and SAED pattern, (L) EDS spectra. B5F5 control: (M) morphology and SAED pattern, (N) EDS spectra.

Ca, calcium; F, fluoride; O, oxygen; P, phosphorus; Sr, strontium; EDS, energy-dispersive X-ray spectroscopy; SAED, selected-area electron diffraction.
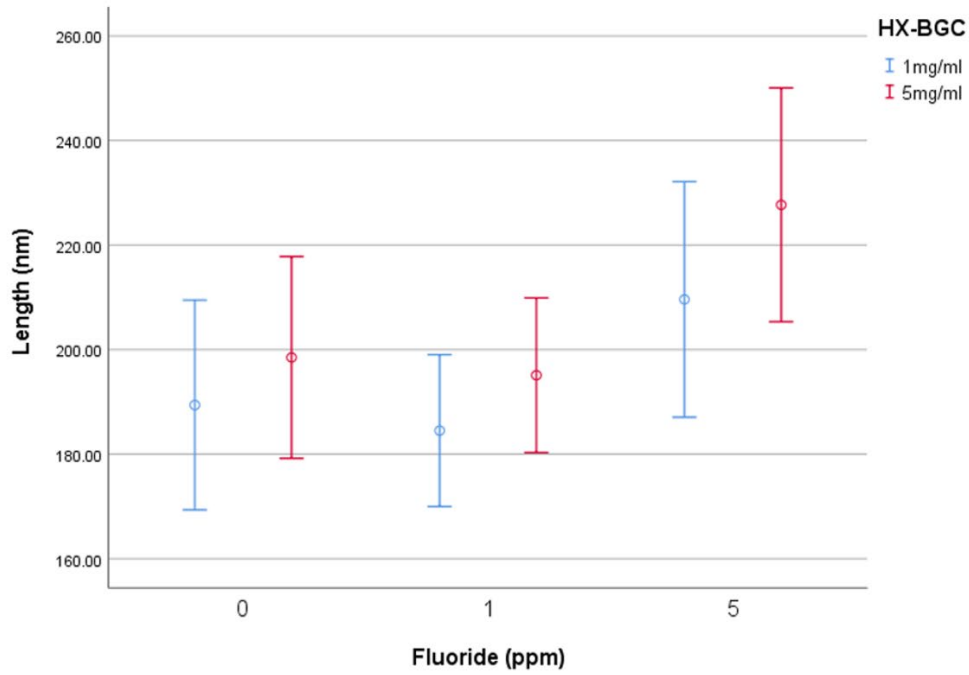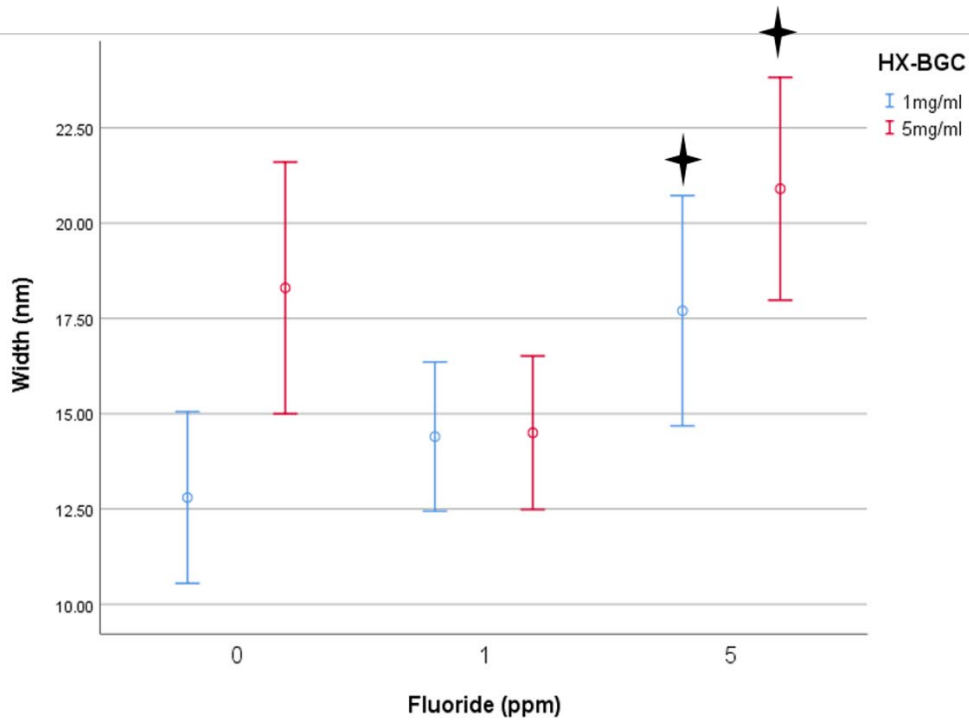
Figure 2. Length (A) and width (B) measurements (average ± SD) of the apatite crystals grown in the presence of the bioactive glass (HX-BGC) and with different concentrations of fluoride (0,1 and 5 ppm). Two-way ANOVA analysis. ✦: $p<0.05$
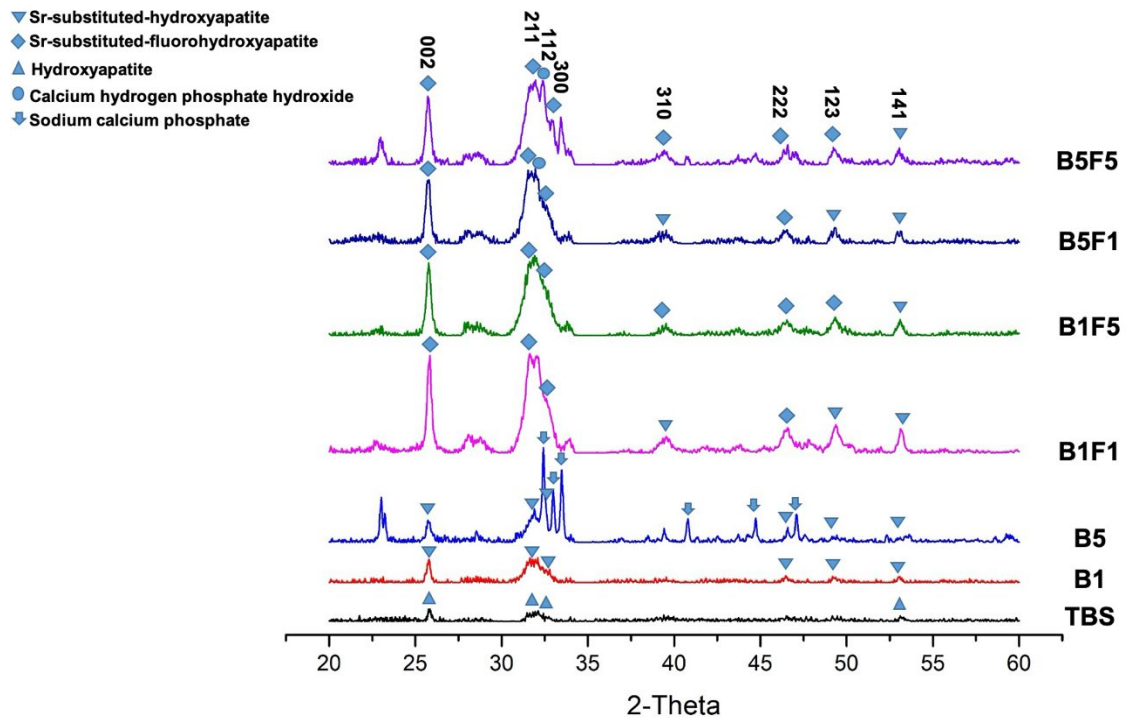
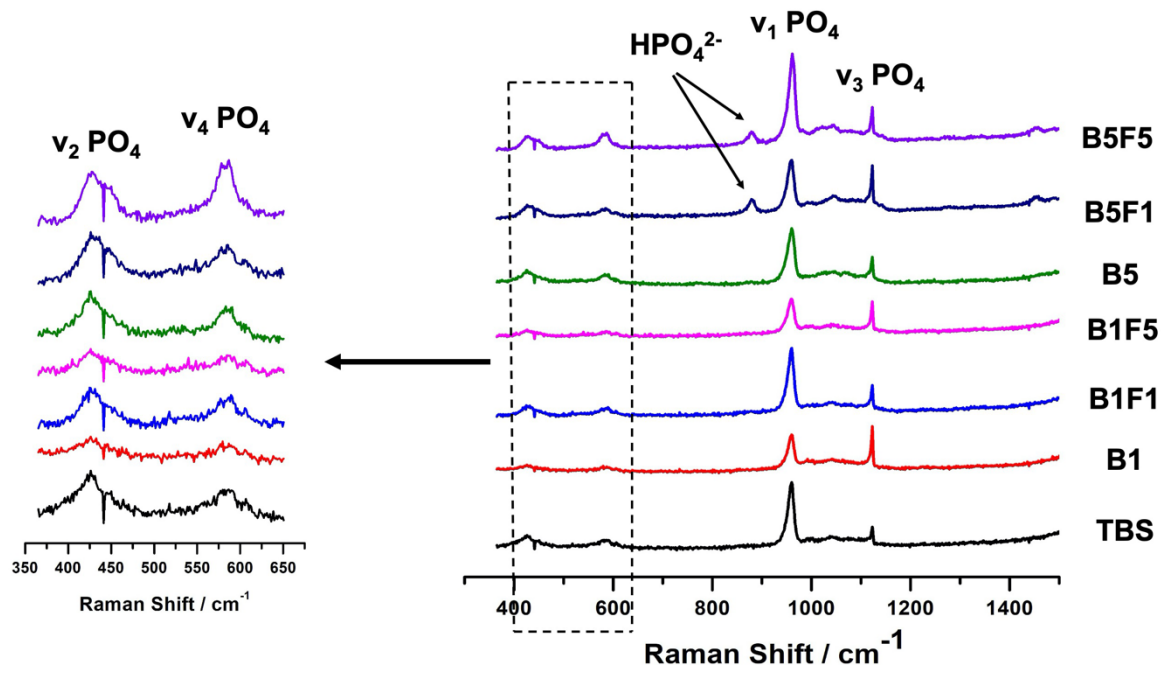Figure 3. Typical powder X-ray diffraction patterns of experimental groups: range 20º to 60º.

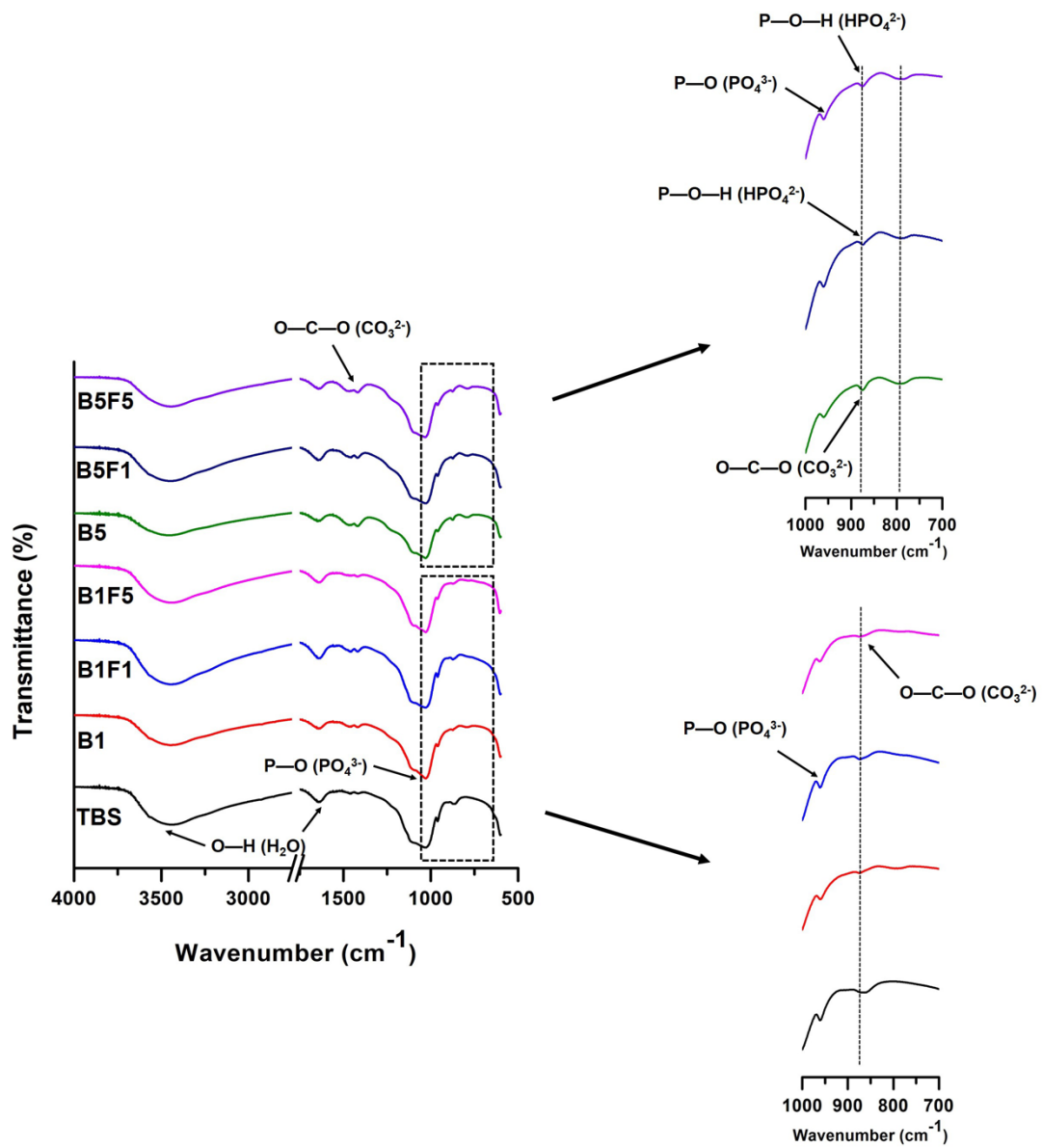Figure 4. Typical Raman spectra of experimental groups: range, 400 -1400 cm^{-1}.

Figure 5. Typical FTIR spectra of experimental groups: range, 500 cm^{-1} to 4000 cm^{-1}.

Table 1. The length and width of apatite crystals evaluated from TEM images.

Group	Length (nm)	Width (nm)
Control (1)	105.9±20.4	5.9±2.6
B1 (2)	189.4±20.1	12.8±2.3
B5 (3)	198.5±19.3	18.3±3.3
B1F1 (4)	184.5±14.5	14.4±2.0
B1F5 (5)	195.1±14.8	14.5±2.0
B5F1 (6)	209.6±22.5	17.7±3.0
B5F5 (7)	227.7±22.4	22.1±3.2
P value	$p < 0.001$	$p < 0.001$
Multiple Comparison	(1)<(2),(3),(4),(5),(6)<(7)	(1)<(2)<(4),(5)<(3),(6)<(7)

All the data are normally distributed. Values are presented as mean ± SD.

TEM, transmission electron microscopy.

Table 2. Calculated hexagonal unit cell parameters *a* and *c* axes, and Ca/P ratio in experimental groups

Group	P-XRD (Å)		Ca/P
	a-axis	*c*-axis	
Control	9.408±0.008	6.862±0.007	1.581±0.097
B1	9.431±0.008	6.877±0.003	1.504±0.022
B1F1	9.419±0.008	6.879±0.001	1.695±0.058
B1F5	9.405±0.009	6.853±0.005	1.796±0.077
B5	9.432±0.001	6.886±0.004	1.809±0.097
B5F1	9.424±0.001	6.878±0.001	1.531±0.038
B5F5	9.372±0.010	6.856±0.001	1.579±0.056

All the data are normally distributed. Values are presented as mean ± SD.

Ca/P, calcium/phosphate. P-XRD, powder X-ray diffraction.